Modeling borehole radar electromagnetic wave propagation in conductive media by implementation of parallel three-dimensional finite-difference time domain technique

Pradip K. Muhkopadhyay[1], Andrew J. Wilkinson[2], Thomas Bennett[2], and Michael R. Inggs[2]

[1]Department of Geology and Geophysics, University of Wyoming, Laramie, WY 82071, USA,

[2]Radar Remote Sensing Group, Department of Electrical Engineering, University of Cape Town, Rondebosch-7001, South Africa

Abstract

Modeling borehole radar electromagnetic wave propagation in three-dimension can be used to better understand the physics of observed responses and it can also provide useful insight into the interpretation of real data sets. We have implemented a 3-D finite difference time domain modeling code using a uniaxial perfectly matched layer (UPML) as a boundary absorber. To reduce the large memory requirements as well as to increase the processing speed, a parallel version of this code has been implemented using Parallel Virtual Machine (PVM) as "middleware" running on a Beowulf-type Linux cluster. Modeling study of cross-well EM wave propagation in a sedimentary layer, EM wave reflection from geological reverse fault and pothole-type structure in a conductive host rock was performed. The borehole is in direct contact with the subsurface host rock, and thus penetrates more than when the antennas are on surface. The radar traces are affected by the presence of borehole, layer thickness and scattering from sharp edges. These effects can be included in a full waveform inversion to better extract information from the amplitudes. When both the antennas are in the same sand layer, the initial travel time of the guided wave equals the initial travel time of the wave in the homogeneous medium. This property can be used to calculate the dielectric permittivity of the medium, which is related to important formation properties such as propagation velocity and water saturation. Our modeling study shows that borehole radar is a useful high resolution imaging tool for both mining as well as oilfield applications.

Introduction

Imaging subsurface structures in three dimensions (3-D) with high resolution is of high importance in the geophysical industry. Borehole radar is a high resolution electromagnetic (EM) sensor which can detect electrical discontinuities in rock formations with high resolution (~1m) (e.g., Mason, et al, 2001; Chen and Oristaglio, 2002). In real borehole radar measurements, the media through which the EM wave propagates are often complex in nature, and the shape of the target orebody also tends to be different from the commonly used ideal models (e.g. point, plane, cylinder and sphere). The penetration depth of this high frequency radar signal into the host rock is a major concern. The response from the host rock may well swamp the return from the orebody. Therefore, before applying this imaging technique for subsurface imaging, it is important to study the propagation of EM waves in such a media. Three-dimensional modeling of EM wave propagation in borehole environment is a useful tool for understanding the physics of observed responses, for data processing (e.g. propagation velocity in wave-field migration) and data interpretation. Another important question is the effect that the drilling fluid, water or air that may be present in the borehole itself will have on coupling from an antenna to the host rock medium.

The finite difference time domain (FDTD) method (Yee, 1966) is a full-wave, dynamic and powerful numerical method for solving Maxwell's equations. The FDTD method is furthermore ideal for modeling transient EM fields in inhomogeneous media. Complex geological and antenna structures fit relatively easily into finite-difference grid, and absorbing boundary conditions can truncate the grid to simulate an infinite region. Finite-difference modeling data provides estimates of the distributions of velocity and the attenuation of EM waves in the media (Wang and McMechan, 2002). Since the method is a time domain one, wideband data are potentially available from a single run.

We have implemented a 3-D FDTD code in a Cartesian coordinate system to simulate the EM field responses of a dipole source in a lossy medium. A uniaxial perfectly matched layer (UPML) has been added at the outer boundary of the simulation space for boundary absorber (Gedney, 1996). A cylindrical borehole has been included in the simulation and the borehole surface is modeled by an average staircase approximation. The FDTD algorithm can be described as a 'single program multiple data' (SPMD) parallel architecture, which means that each process executes the same program. In order to overcome the problems of large memory requirements and processing speed limits, a parallel version of the 3-D FDTD code has been designed and implemented by using PVM as "middleware" running on a Beowulf-type Linux cluster (Bennett, 2001; Mukhopadhyay, 2006).

This parallel 3-D FDTD simulator has been used for subsurface imaging, such as, layered sediments EM wave propagation, EM wave reflection from geological reverse fault and pothole type structure in conductive host. In layered sediments, when the wavelength of the propagating pulse is similar to the thickness of the host layer; cross-well radar

traces start propagating as a guided wave. The initial travel time of the guided wave remains the same as that with the wave of homogeneous model (Ellefsen, 1999 and Mukhopadhyay, 2006). A cylindrical borehole has been included in the simulation and the effect of borehole, layer thickness and scattering from sharp edges on radar traces has been discussed.

Numerical Method: Parallel Processor Implementation

The Radar Remote Sensing Group's (RRSG) has a Beowulf Cluster called Gollach which was the hardware benchmark for this work. The cluster hardware specifications are: one dual-CPU Intel Pentium II, 350 MHz, with 256 MB RAM and two single-CPU Intel Pentium II, 350 MHz, with 256 MB RAM per machine. The machines were connected to each other via a Fast Ether-Net 100 Mb switch.

The FDTD algorithm best fits into Flynn's taxonomy (Bennett, 2001) of parallel computers, as a single program multiple data (SPMD) type architecture. The slave processes behave according to set parameters, depending upon the sources, boundary conditions and material properties. Figure 1 shows the program flow of the parallel FDTD software implementation. The 3-D FDTD computational grid is divided approximately equally between the slave processes, so that each slave process has an identical processing load, which leads to this parallel FDTD algorithm to be efficient. Attention needs to be paid for source and receiver locations; they should not fall at the process boundary. The master process has been used for initialization of the slave processes only. The slave processes need to communicate with each other when they are at the data boundaries. This 2-D interface data, H-field and E-field are packed and communicated between the slave processes by using routines from the PVM library. The data are sent and received using the pvm_send() and pvm_recv() routines.

Both the FDTD serial and parallel algorithms have been implemented successfully. A speed up of 2.7 is achieved, which corresponds to a 90% efficiency, where a speed of 3 for three slave processors is considered to be of 100% efficiency.

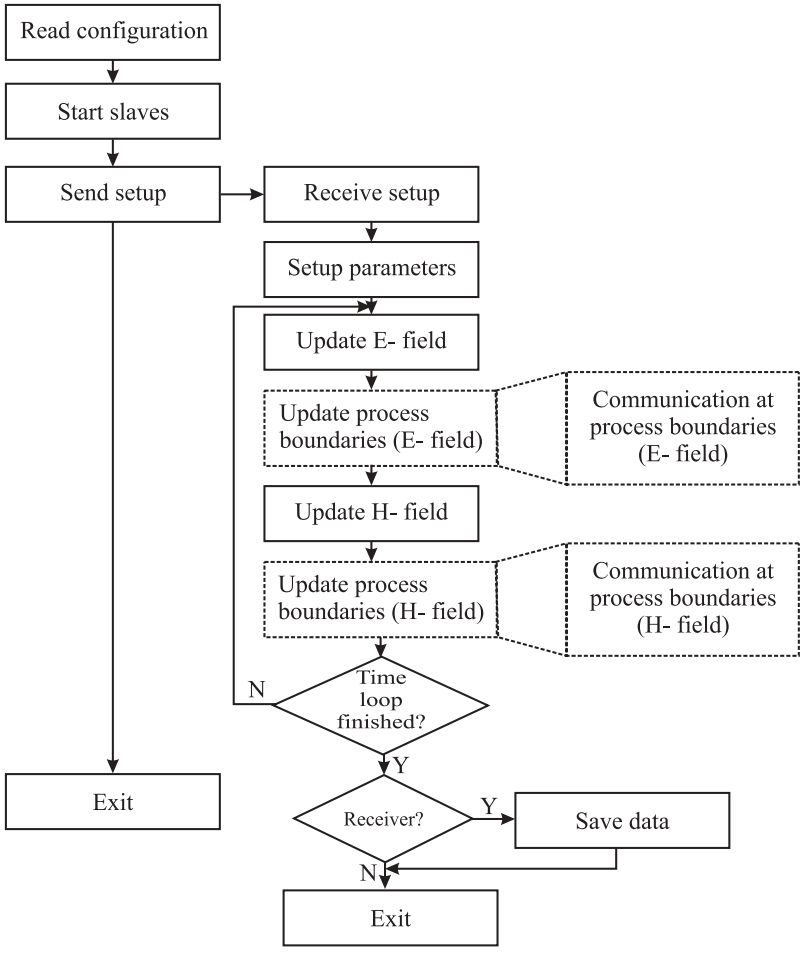

Fig. 1 Design of FDTD parallel processor program flow. Master process is used for initialization of the slave processes. Slave processes needs to communicate each other at the boundary.

Due to CPU memory and speed limitations and the fact that there were only three nodes in the Gollach cluster, the speed up tests was limited to a small data set. However, we note that if the size of the data set increases, the network load will scale up proportionately, and will consequently degrade the efficiency. Figure 2(a) shows the improvement of the processing time between a serial and parallel processor as a function of number of time steps for a same volume of computational space. Figure 2(b) shows the efficiency of the parallel processor in the three node Gollach cluster. The ideal case would have an efficiency of 100% for any number of processes. The performance of this parallel processor will deteriorate as the number of processes increases and the communication time becomes larger. Figure 2(c) shows the XPVM printout of the CPU utilization, where green indicates computing and red indicates waiting on communication. The interpretation of this is that most of the processing time on the cluster is taken up with processing the data and thus the parallel algorithm utilizes the available computing resources efficiently.

Application of parallel 3-D FDTD modeling technique for subsurface imaging

In all the simulation experiments, transmitting antenna is simulated by a vertical electric dipole with infinitesimal length. The source wavelet is the first derivative of the Blackman-Harris window function (Harris, 1978; Chen et al, 1997). The co-efficients used here are slightly different from the original Blackman-Harris window function to make

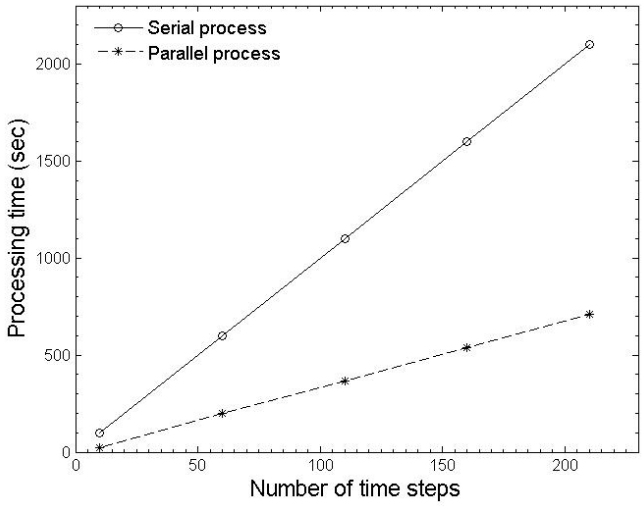

(a)

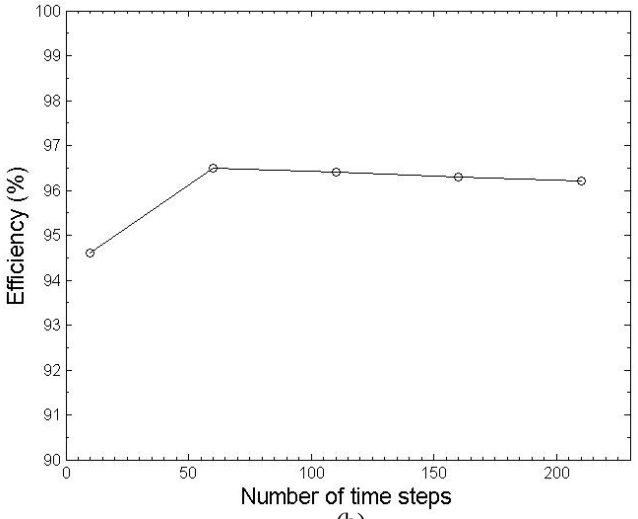

(b)

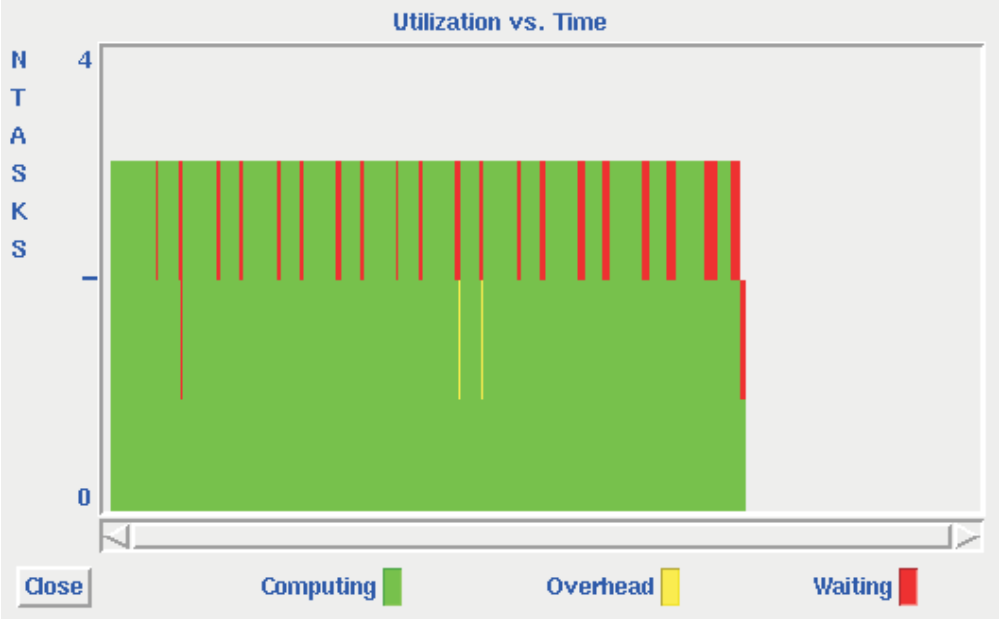

(c)

Fig. 2 Parallel 3-D processor, (a) Serial vs parallel processing time (b) Efficiency vs processing time (c) CPU utilisation in the parallel process.

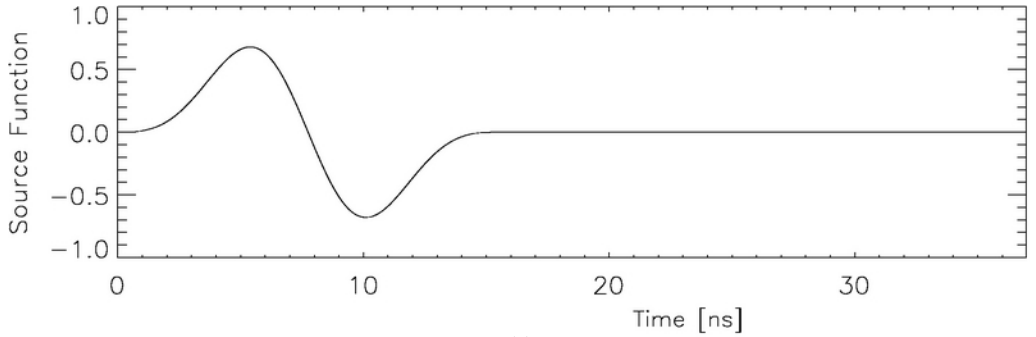

(a)

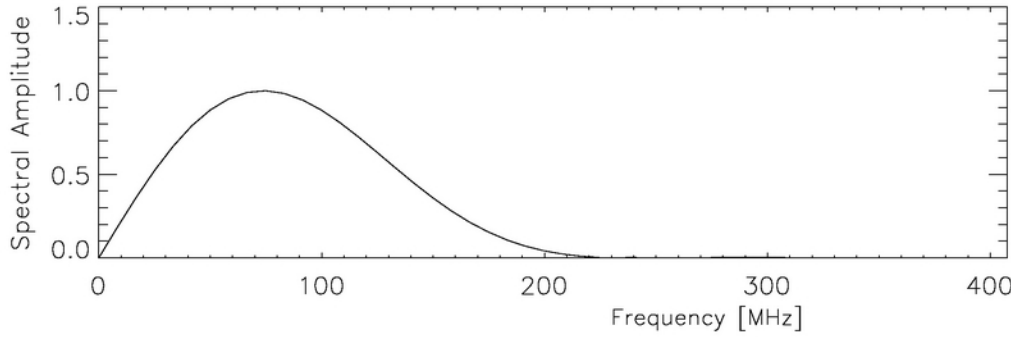

(b)

Fig. 3 The first derivative of the Blackman-Harris window function used as the incident field. (a) Pulse shape in time domain (b) Pulse shape in frequency domain with a nominal frequency of 100 MHz.

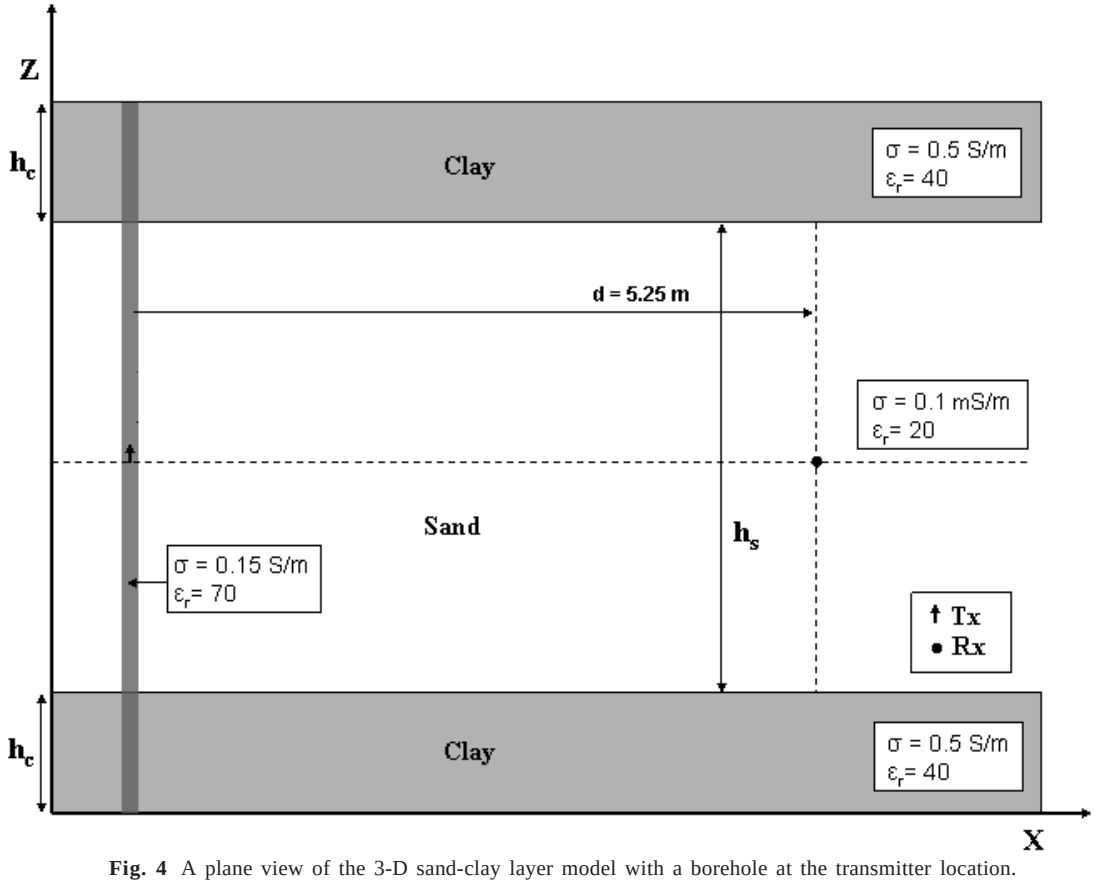

Fig. 4 A plane view of the 3-D sand-clay layer model with a borehole at the transmitter location.

the pulse vanish completely after time period of the pulse (Chen et al, 1997). The source wavelet and the spectrum of the pulse with nominal frequency of 100 MHz and a centre frequency of around 80 MHz are shown in Figure 3. As the FDTD modeling code was implemented in Cartesian coordinate system, the cylindrical borehole surface was modeled by an average staircase approximation. The ten cell thick PML (UPML) layer has been used in all the simulation as boundary absorber and the simulation space has been digitized with same grid size in each simulation experiment. At the receiver location, either the axial electric field or the transverse magnetic field was recorded.

Example 1: Layered sediment cross-well electromagnetic wave propagation study

Often in near surface geological setting, the sedimentary rocks are layered with sand and clay sequence and it is useful to study the borehole radar responses in such a geological configuration. Figure 4 shows the plane view of a 3-D sedimentary layer with a dimension of (x,y,z) = (7.0,2.2,4.5)m. The top and the bottom layers are clay layers and the middle layer represents a sand layer with a height of $\mathbf{h}_s$. The electrical properties are mentioned in the figure. A borehole of 64 mm diameter was placed along the Z-axis at (x,y) = (0.5,1.1)m and the borehole mud was modeled as wet clay. The transmitting and receiving locations were placed in the middle of the sand layer at (x,y,z) = (0.5,1.1,2.2)m and (x,y,z)=(5.75,1.1,2.2)m respectively. The source function (a Blackman-Harris window function) with a nominal frequency of 100 MHz was added to the Ez component at the source location at each time step. The problem space was sampled with the uniform grid size of 0.016m.

Figure 5(a) shows the received radar traces (Ez) in the middle of the sand layer with the sand layer thickness $\mathbf{h}_s$ = 4.0m and with a transmitter-receiver distance of d = 5.25 m, with and without a 64mm diameter borehole at the transmitter location. Three different types of waves are clearly visible in the layered media radar traces, the direct wave, first reflected wave and the second reflected wave. The signature of the radar traces, with and without the borehole, is different. A very small time delay is observed, which is due to the low velocity of borehole mud.

In the case, without the borehole, the two positive peaks of the direct wave are almost similar to each other. However, in the trace with the borehole, the first positive peak of the direct wave is much larger than the next one. This is perhaps the borehole mud has different electrical properties than the host material (sand layer) and there will be multiple reflections at the boundary between the borehole and the sand layer. These reflections will interfere with the transmitting pulse, and consequently will reshape the travelling wave (which acts as a filter in the frequency domain). Therefore, the amplitude of the direct wave, in the presence of the borehole, is not as symmetric as the one without the borehole (dotted curve in Figure 5(a)).

Moreover, the amplitude of the trace with the borehole is larger than that of the trace without the borehole. The borehole mud has a lower impedance ($Z=\sqrt{(\mu/\varepsilon)}$; $\varepsilon_r=70$) than the host material ($\varepsilon_r=20$). The first impression is that more power has been launched into the medium than in the previous case. The increase in amplitude, through, is not simply the result of lower impedance. As we are not modeling the antenna configuration in this work, we can't directly discuss the effect of antenna impedance. When the material has finite conductivity, the intrinsic impedance is a complex number. The dielectric constant will have more effect on the antenna impedance, and the conductivity will affect the absorption of the energy radiated from the antenna. In this simulation, we kept the E-field strength constant, but in a real situation, a more realistic condition would have to be considered. For instance, the open voltage applied to the antenna would need to be kept constant, independently of the surrounding material. The input impedance of the antenna will strongly be influenced by the surrounding material, and the impedance matching condition will also change. Therefore, the power radiated into the medium is a function of the input impedance of the antenna, which can be studied once a proper antenna configuration will be included in the simulation work.

To analyze the effect of borehole mud conductivity on radar traces, both the traces with varying the borehole mud conductivity are normalized by their corresponding received power, as shown in Figure 5(b). In this case, too, the change is not significant. The effect of attenuation on the received radar trace (in case of high conductive mud, dotted trace) is more significantly pronounced in the later stage of the received trace rather in the earlier stage. This may be because of the multiple reflected waves in the borehole are affected by the high attenuation caused due to more conductive borehole mud.

Figure 5(c) shows a comparison between the radar traces recorded by using the borehole only at the transmitting location and then at both the transmitting and the receiving location. The signatures of both traces are similar. Nonetheless, there are some time differences with regard to the time of arrival. This is because, in the former case, the pulse travels a smaller distance through the borehole mud, where the velocity of propagation is less. The amplitude of the latter trace is thus slightly higher than that of the former. This may be due to internal reflection from the borehole wall and also due to the different electrical conductivity of the borehole mud and the host medium.

Figure 5(d) shows the received radar trace in the middle of the sand layer at a transmitter-receiver distance of d=5.25 m. The sand-layer thickness is $\mathbf{h}_s$=1.0 m and a 64mm diameter borehole is located at the transmitter location. In this case, however, the thickness of the sand layer is close to the significant wavelength (3-dB point) of the transmitting

pulse (the wavelengths in sand layer are between 0.4 and 1.3 m at corresponding frequencies of 175 and 50 MHz), and thus all reflected waves are superimposed on the direct wave and thus form the guided wave. The superposition of the reflected waves on the direct wave will cause interference. The amplitude of the guided wave will thus either increase or decrease, depending on the relative path lengths between the direct wave and the reflected wave, which is a function of the sand layer thickness. The same trace has been compared with a trace from homogeneous model. The initial travel time of both the traces is same. The initial travel time can be used to determine the dielectric permittivity of the medium by using the relationship of phase velocity (v) and dielectric permittivity (ε_r) [$v = c/\sqrt{\varepsilon_r}$; c is the velocity of light in air]. This dielectric permittivity can be utilized to calculate the formation properties such as water saturation of the medium.

Example 2: Borehole radar EM wave reflection from geological reverse fault in a conductive host rock

A reverse fault is a dip-slip fault where the rock above the fault plane (hanging wall) has moved upward relative to the rock below the fault plane (foot wall). Bodies of rock which are compressed horizontally thus often contain reverse fault. Figure 6 shows the plane view of a 3-D reverse fault in a conductive host rock. The electrical properties are indicated in the figure. The same source function with a nominal frequency of 70 MHz, was added to the Ey component at the transmitter location on the Y-axis and the transverse magnetic field component Hx at a constant interval of 0.5 m along the Y-axis was recorded. The data was collected with a common source gather mode which is called as wide-angle reflection and refraction (WARR) sounding.

Figure 7(a) shows the reflected waveform resulting from the hanging wall and foot wall of the fault surface. The direct waves have been removed from the recorded waveform. The existence of a reverse fault in the conductive host, as indicated by the hanging wall and the foot wall surface, is clearly visible in the reflected waveform. The amplitude of the waveform reflected from the hanging wall is greater than the waveform reflected from the foot wall. This is due to the loss of energy of the waveform in the conductive host and also energy lost due to spherical spreading. Figure 7(b) shows

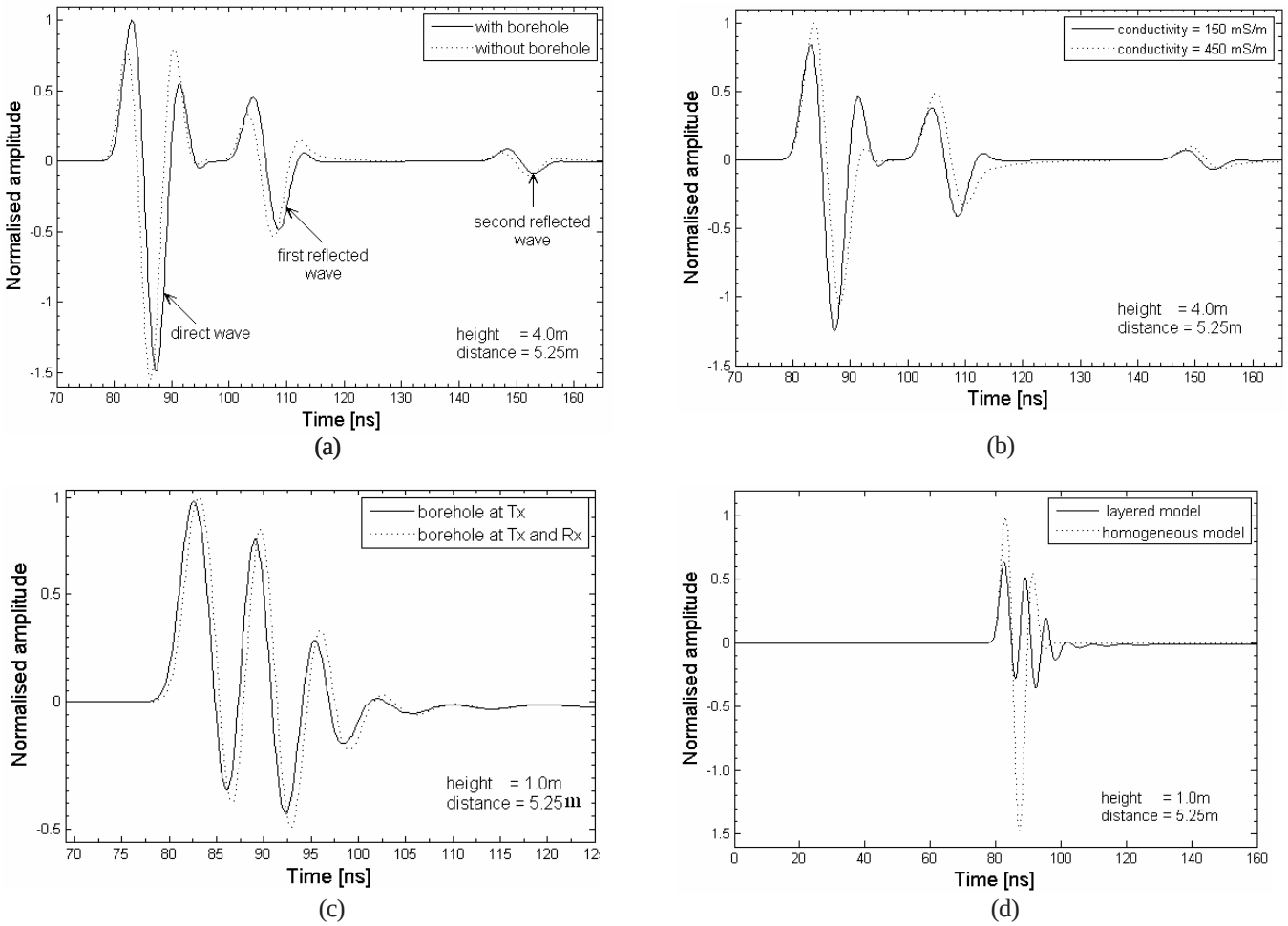

Fig. 5 Cross-well radar traces (a) effect of borehole on radar traces, (b) effect of conductivity of the borehole mud on radar traces, (c) effect of borehole at transmitting location and both transmitting and receiving location, (d) effect of layer thickness on radar traces.

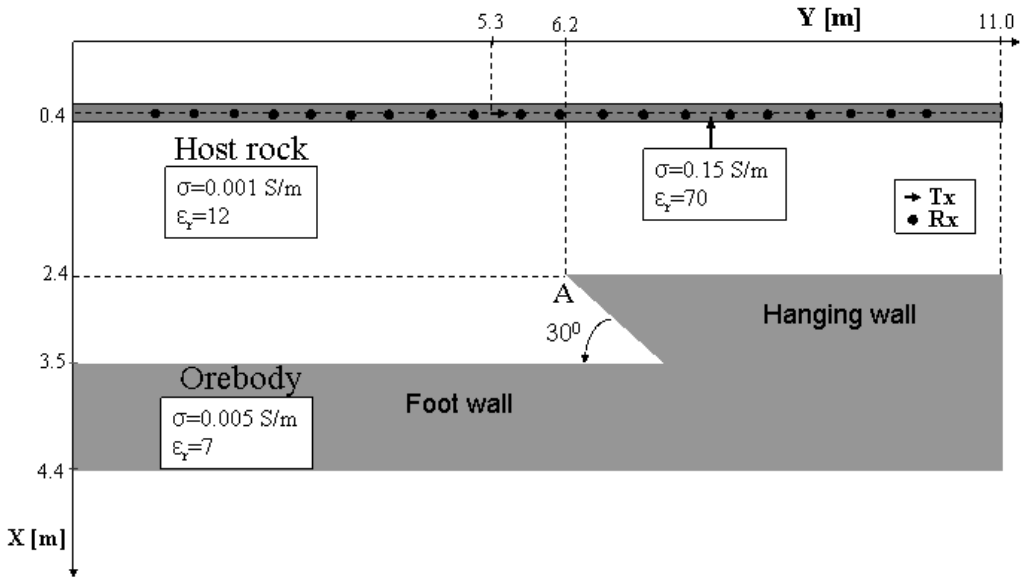

Fig. 6 A plane view of the geological reverse fault with a borehole at the transmitting and receiving end. The transmitter is located inside the borehole at Y = 5.3m.

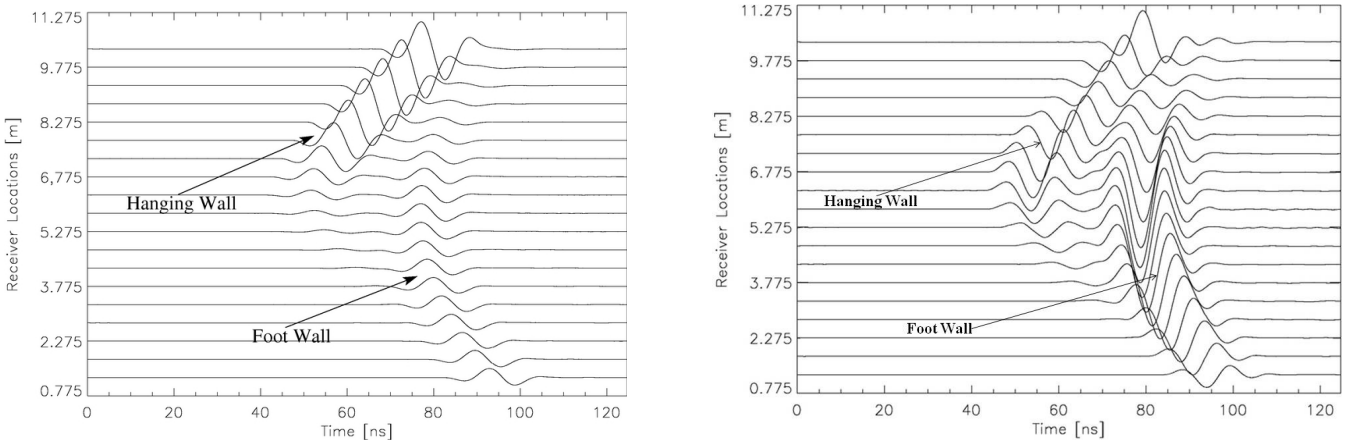

Fig. 7 Reflected waveform from the hanging wall and the fool wall of the reverse fault. The direct waves have been removed from the recorded waveform. (a) Reflected waveform without a borehole and (b) Reflected waveform with a borehole of 100mm diameter at the transmitting and receiving location.

the reflected waveform from the same fault surface, but in this case the transmitting and receiving antenna are inside a 100mm borehole.

Figure 8 shows the radar traces recorded at three different locations in the borehole, one at the hanging wall side (Figure 8(a)), next close to the sharp edge (Figure 8(b)) and the other is at the foot wall side of the reverse fault (Figure 8(c)). The traces have been compared with traces reflected from the same height in absence of fault surface. The scattering from the sharp edge of the reverse fault (marked A in Figure 6), however, does interfere noticeably with the reflected wave from the hanging wall at the start of the traces (near point A), although, as one moves further along the receiver path, the effect becomes minimal, as we can see from the fact that the amplitude increases away from the sharp edge discontinuity (as shown in Figure 8).

Example 3: Imaging Pothole-type structure in a conductive host rock

A pothole-type structure is defined as a semispherical hole in the bedrock of a stream bed, formed by abrasion of small pebbles and cobbles in a strong current. Figure 9 shows a plane view of the 3-D geological model used in this simulation experiment. A common offset data acquisition mode was used where the distance between transmitting and receiving location was kept fixed at 0.25m. Other parameters used were dd = 4.5m, h = 2.0m and d = 1.5m. In this experiment, 70MHz source function was added to the

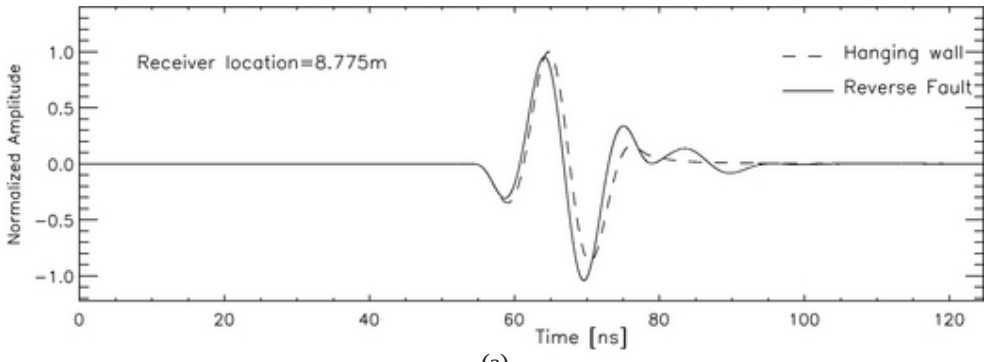

(a)

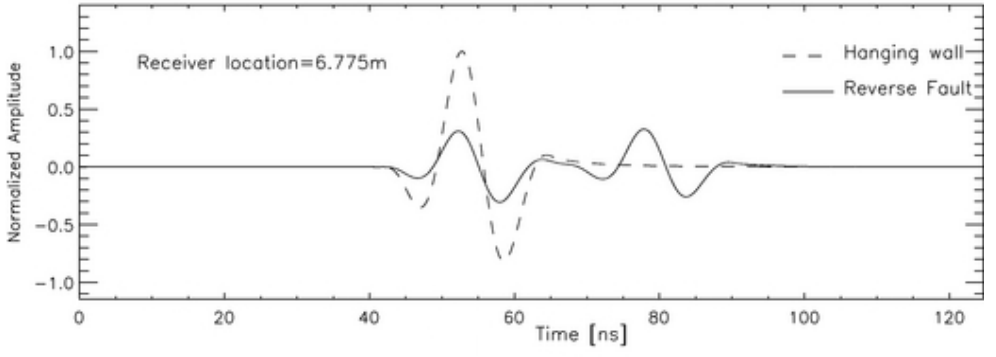

(b)

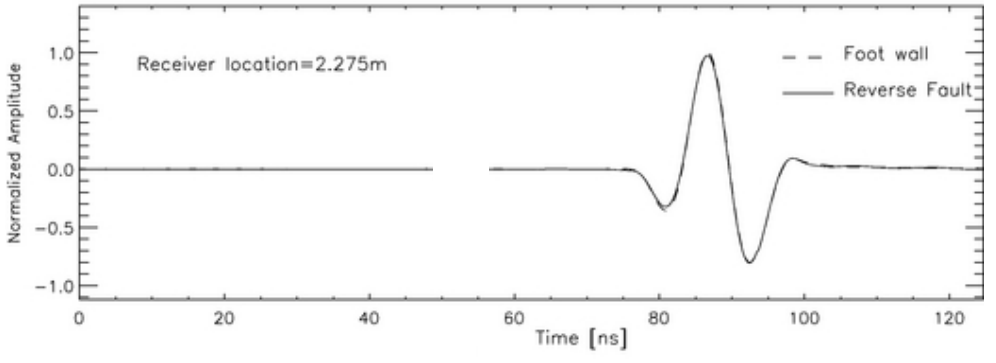

(c)

Fig. 8 Effect of scattering from the sharp edge (marked as A in Figure 6) on radar traces. (a) Received traces on the hanging wall side, (b) Traces close to A, and (c) Traces on the foot wall side. All the traces were compared with traces from surfaces without any sharp discontinuity.

Ex component and the vertical component of the electric field Ex has been recorded. A borehole of 100mm diameter was added at the transmitting and receiving location. The curved pothole structure was modeled by a staircase approximation.

Figure 10 shows the recorded waveform with automatic gain control function applied. The presence of pothole type structure is visible in the recorded waveform in presence of strong direct wave. The exact shape of the orebody can be found after applying proper migration technique on the received data. Figure 11 shows the recorded waveform from the same geometry, but in this case the conductivity of the host rock was increased to 5.0 mS/m. Due to high conductivity of the host rock, the amplitude of the waveform decreases and the reflection from the pothole

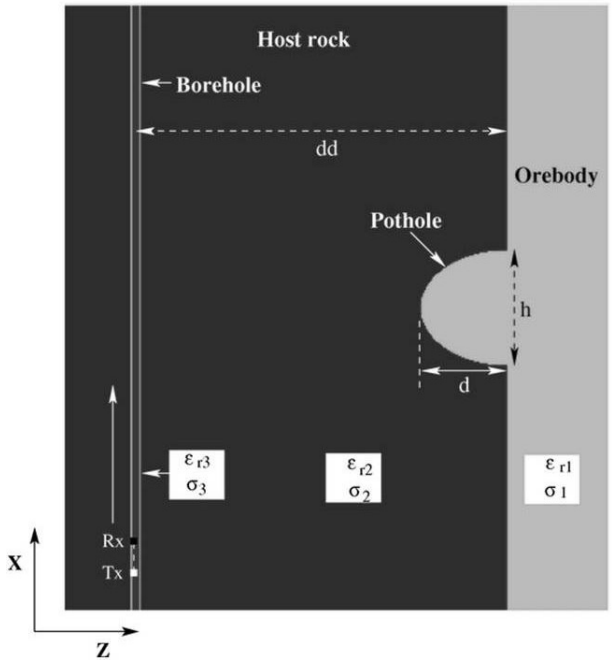

Fig. 9 A plane view (X-Z) of the 3-D pothole-type structure embedded in a conductive host rock with a borehole of diameter 100mm at the transmitting and receiving location. The data has been recorded with a common offset data acquisition mode.

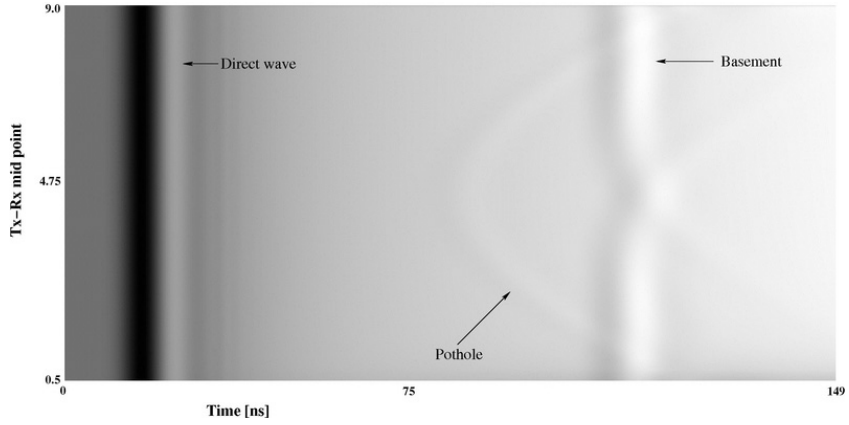

Fig. 10 A gray scale display of the received radar traces. Automatic gain control function has been applied to the received traces. The conductivity of the host rock is modeled as 0.05 mS/m.

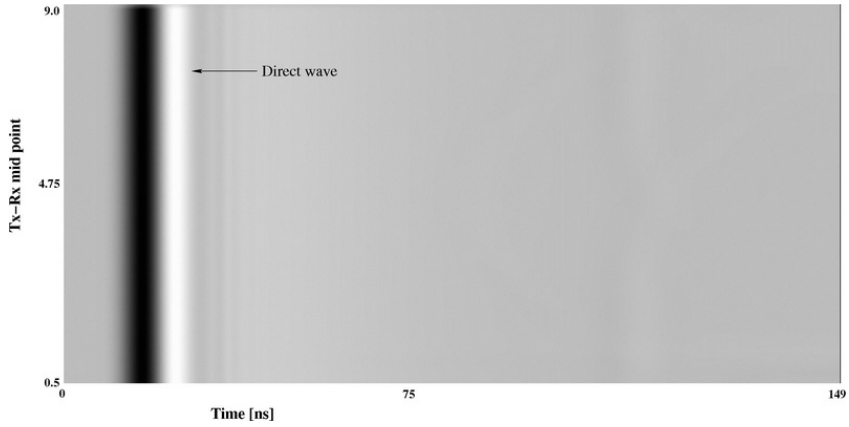

Fig. 11 A gray scale display of the received radar traces. Automatic gain control function has been applied to the received traces. The conductivity of the host rock is modeled as 5.0 mS/m.

structure was not visible.

Conclusions

We have developed a parallel FDTD modeling code for EM wave propagation. A parallel 3-D FDTD simulator does reduce the processing speed as well as the memory requirement compared to a serial 3-D FDTD simulator. Although, the communication time overhead becomes larger with a large number of processes. Our modeling study demonstrates that borehole radar can be useful for mining as well as oilfield applications for imaging electrical discontinuity with high resolution.

In case of layered media EM wave propagation, a guided wave starts propagating when the thickness of the sand layer is similar to the pulse wavelength. The amplitude of the propagating wave varies with the thickness of the sand layer, but the initial travel time remains the same compared to the wave from homogeneous model. This property can be utilized to estimate the dielectric permittivity of the medium. The effect of borehole on radar traces has been noticed; the shape, signature and the initial travel time of the received waveform changes. The power radiated into the medium is a function of the input impedance of the antenna, which can be studied once a proper antenna configuration is included in the simulation work. The scattering from the sharp edge of the orebody interferes with the reflected waves and does increase or decrease the amplitude of the received wave depending upon the relative path length. As the conductivity of the host rock increases and, hence, intrinsic attenuation increases, the amplitude of the reflected wave decreases. These findings can be included into a full-waveform inversion to extract better information from amplitude.

References

Bennett, T., 2001, Development of a parallel SAR processor on a Beowulf cluster, M.Sc Thesis, University of Cape Town, South Africa.

Chen, Y. H. and Oristaglio, M. L., 2002, A modeling study of borehole radar for oil-field applications, Geophysics, 67(5), 1486-1494.

Chen, Y.-H., Chew, W.C., and Oristaglio, M.L., 1997, Application of perfectly matched layers to the transient modeling of subsurface problems, *Geophysics*, 62(6), 1730–1736.

Ellefsen, K. J., 1999, Effects of layered sediments on the guided wave in cross-well radar data, *Geophysics*, 64(6), 1698-1707.

Gedney, S. D., 1996, An Anisotropic Perfectly Matched Layer-Absorbing Medium for the Truncation of FDTD Lattices, *IEEE Trans. on Antennas and Propagation*, 44, 1630-1639.

Gedney, S. D., 1996, An Anisotropic PML Absorbing Media for FDTD Simulation of Fields in Lossy Dispersive Media, *Electromagnetics*, 16, 399-415.

Harris, F. J., 1978, On the use of windows for harmonic analysis with the discrete Fourier transform, *Proc. IEEE*, 66, 51-83.

Mason, I., Osman, N., Liu, Q., Simmat, C., and Li, M., 2001, Broadband Synthetic Aperture Borehole Radar Interferometry, *Journal of Applied Geophysics*, 47, 299–308.

Mukhopadhyay, P. K., 2006, Three-dimensional Borehole Radar Imaging, PhD Thesis, University of Cape Town, South Africa.

Wang, D. and McMechan, G.A., 2002, Finite-difference modeling of borehole ground penetrating radar data, *Journal of Applied Geophysics*, 49, 111–127.

Yee, K. S., 1966, Numerical solution of initial boundary value problems involving Maxwell's equations in isotropic media, *IEEE Trans. on Antenna and Propagation*, AP-14(3), 302-307.